Human Molecular Genetics, 2011, Vol. 20, No. 3 ***422–435***
doi:10.1093/hmg/ddq478
Advance Access published on November 3, 2010

Lack of WDR36 leads to preimplantation embryonic lethality in mice and delays the formation of small subunit ribosomal RNA in human cells *in vitro*

Martin Gallenberger[1,†], Dominik M. Meinel[1,†,‡], Markus Kroeber[1], Michael Wegner[3], Philipp Milkereit[2], Michael R. Bösl[4] and Ernst R. Tamm[1,*]

[1]Institute of Human Anatomy and Embryology and [2]Institute of Biochemistry, University of Regensburg, Universitätsstr. 31, 93053 Regensburg, Germany [3]Institute of Biochemistry, Emil-Fischer-Centre, University of Erlangen-Nürnberg, Germany and [4]Max Planck Institute of Neurobiology, Martinsried, Germany

Received September 8, 2010; Revised and Accepted November 1, 2010

Mutations in WD repeat domain 36 gene (*WDR36*) play a causative role in some forms of primary open-angle glaucoma, a leading cause of blindness worldwide. WDR36 is characterized by the presence of multiple WD40 repeats and shows homology to Utp21, an essential protein component of the yeast small subunit (SSU) processome required for maturation of 18S rRNA. To clarify the functional role of WDR36 in the mammalian organism, we generated and investigated mutant mice with a targeted deletion of *Wdr36.* In parallel experiments, we used RNA interference to deplete WDR36 mRNA in mouse embryos and cultured human trabecular meshwork (HTM-N) cells. Deletion of *Wdr36* in the mouse caused preimplantation embryonic lethality, and essentially similar effects were observed when WDR36 mRNA was depleted in mouse embryos by RNA interference. Depletion of WDR36 mRNA in HTM-N cells caused apoptotic cell death and upregulation of mRNA for BAX, TP53 and CDKN1A. By immunocytochemistry, staining for WDR36 was observed in the nucleolus of cells, which co-localized with that of nucleolar proteins such as nucleophosmin and PWP2. In addition, recombinant and epitope-tagged WDR36 localized to the nucleolus of HTM-N cells. By northern blot analysis, a substantial decrease in 21S rRNA, the precursor of 18S rRNA, was observed following knockdown of WDR36. In addition, metabolic-labeling experiments consistently showed a delay of 18S rRNA maturation in WDR36-depleted cells. Our results provide evidence that WDR36 is an essential protein in mammalian cells which is involved in the nucleolar processing of SSU 18S rRNA.

INTRODUCTION

Glaucoma, the second leading cause of blindness worldwide (1), is a chronic, degenerative optic neuropathy characterized by a progressive degeneration of optic nerve axons leading to typical visual field defects (2). In the most common form, primary open-angle glaucoma (POAG), the resistance to outflow of aqueous humor increases in the trabecular meshwork outflow pathways, a condition that leads to an increase in intraocular pressure (IOP) (3,4). In several prospective, randomized, multicenter clinical studies, IOP has been identified as the most critical risk factor for the development of optic nerve axonal damage in POAG (5–10). The neurotrophin hypothesis of POAG proposes that abnormally high IOP causes an obstruction of retrograde transport in optic nerve axons at the optic nerve head, a scenario that results in the deprivation of neurotrophic support to retinal ganglion cells (RGC) leading to their apoptotic cell death and to vision loss (11,12).

Susceptibility to POAG may be inherited as a Mendelian trait, or, probably in most cases, may depend on complex trait inheritance resulting from interactions of multiple genetic factors and the influence of environmental exposures (13,14). To date, at least 14 loci (GLC1A to GLC1N) that contribute to the susceptibility of POAG have been localized, and three genes have been identified within these loci: myocilin

*To whom correspondence should be addressed. Tel: +49 9419432839; Fax: +49 9419432840; Email: ernst.tamm@vkl.uni-regensburg.de
†Both authors contributed equally to this study.
‡Present address: Department of Biochemistry, Gene Center and Center for Integrated Protein Science, University of Munich, Germany.

(*MYOC*) (15), optineurin (*OPTN*) (16) and the WD repeat domain 36 gene (*WDR36*) (17). Mutations in *MYOC* were reported in 3–5% of patients with adult-onset POAG and in ~20% of patients with juvenile POAG (18,19). *MYOC* encodes myocilin, a secreted protein with high expression in the trabecular meshwork. Neither the function nor the role of myocilin in the pathogenesis of POAG has been identified (20–22). Mutations in optineurin, a Golgi-associated protein (23–25), are rare events and are found at a frequency of <1% in POAG patients (13,14). Sequence variants in *WDR36* have been identified in the GLC1G locus mapped to 5q22.1 (17). Subsequent studies have confirmed the presence of several non-synonymous *WDR36* sequence alterations exclusive to POAG patients, but also a considerable number of variants in normal controls (26–33). In addition, patients with *WDR36* sequence variations were reported to be associated with a more severe disease phenotype than those without (29). Overall, the available data suggest that *WDR36* plays a role as glaucoma-modifier gene that is involved rather in disease susceptibility than in causation (13,14). Such a role may not be confined to POAG as more recent studies identified *WDR36* sequence variants in patients with high numbers of eosinophil leukocytes associated with allergic disorders such as atopic asthma or pediatric eosinophil esophagitis (34,35).

WDR36 is expressed in multiple ocular and non-ocular tissues, and high amounts of its mRNA have been detected in the heart, skeletal muscle, pancreas, liver and placenta (17). The structural hallmark of WDR36 is the presence of multiple WD40 repeats which are conserved structural motifs of ~40 amino acids that often terminate in a tryptophan-aspartic acid (WD) dipeptide. WD40 repeat proteins have been implicated in a wide variety of cellular functions, such as cell division, cell fate determination, gene transcription, transmembrane signaling, mRNA modification and vesicle fusion (36,37). The underlying common function of all WD repeat proteins is to coordinate multi-protein complex assemblies, where the repeating units serve as a rigid scaffold for protein interactions (36,37). According to a computed protein structure, WDR36 contains 14 WD40 repeats which fold into two connected seven-bladed β-propellers (38). The primary structure of WDR36 shows similarity to that of Utp21 (38), an essential nucleolar ribonucleoprotein in the yeast *Saccharomyces cerevisiae*. Utp21 is part of the small subunit (SSU) processome (39), a large ribonucleoprotein complex containing >40 proteins, which is required for the maturation of the 18S rRNA of the SSU of the ribosome (40). Data reported in a recent study (41) suggest a similar function for Wdr36 in zebrafish, as Wdr36 is ubiquitously expressed in zebrafish, localizes to the nucleolus and loss-of-function phenotypes result in reduced levels of 18S rRNA.

To clarify the functional role of WDR36 in the mammalian organism, we generated mutant mice with a targeted deletion of *Wdr36*. In the present study, we report that the loss of WDR36 in mice leads to preimplantation embryonic lethality. Essentially, similar effects are observed when WDR36 mRNA is depleted in mouse embryos by RNA interference, while depletion of WDR36 mRNA in human cells *in vitro* causes apoptotic cell death. In parallel pulse-chase-labeling experiments, we show that knockdown of WDR36 expression results in a delay of 18S rRNA processing and provides evidence that WDR36 is involved in the formation of SSU rRNA in mammalian cells.

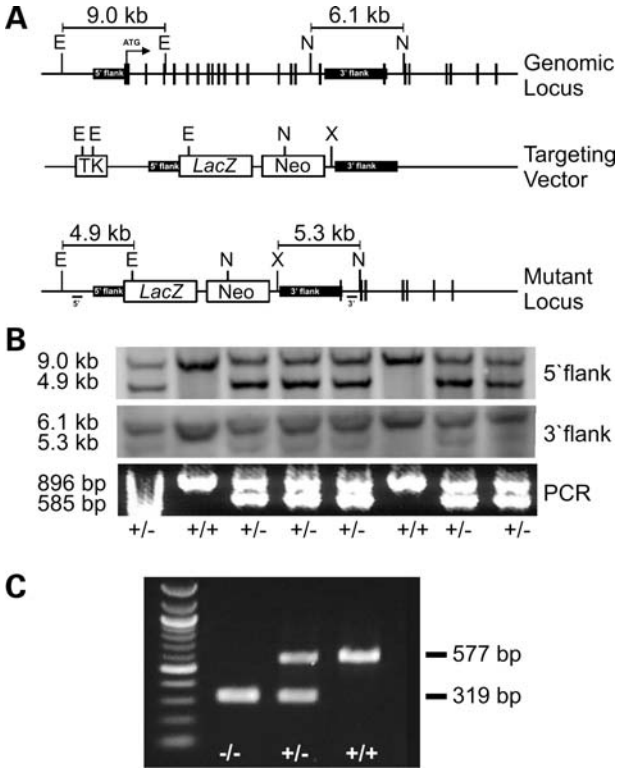

Figure 1. Generation of *Wdr36* null mice. (**A**) Schematic representation of the mouse *Wdr36* genomic locus and the targeting strategy. The targeted disruption results in removal of the first 16 exons of *Wdr36* and generates 4.9 kb *Eco*RV (E) and 5.3 kb *Nco*I/*Xho*I (N, X) fragments when hybridized with 5′ and 3′ Southern probes, respectively. (**B**) Southern blot (upper two panels) or PCR genotype (lower panel) of tail DNA from a representative litter following mating of heterozygous *Wdr36*-deficient animals. A 585 bp PCR fragment is specific for the mutant locus which replaces the wild-type locus normally detected as 896 bp fragment. (**C**) Nested PCR using as template DNA from embryos following mating of heterozygous *Wdr36*-deficient animals. A 319 bp fragment is specific for the mutant locus which replaces the wild-type locus normally detected as a 577 bp fragment.

RESULTS

Targeted removal of *Wdr36* leads to early embryonic death

For gene deletion, we replaced the first 16 exons of *Wdr36* with a lacZ-floxed pgk-neomycin cassette as described in Materials and Methods (Fig. 1A). Following germ-line transmission, genotyping of newborn pups was performed by Southern blot hybridization or PCR. Only heterozygous $Wdr36^{+/-}$ mice or wild-type littermates were detected, strongly indicating that a complete deletion of *Wdr36* is lethal during prenatal development (Fig. 1B). Next, heterozygous *Wdr36*-deficient mice were crossed with each other to obtain preimplantation embryos for genotyping. By using a nested PCR approach, we were now able to detect $Wdr36^{-/-}$ embryos, in addition to embryos with $Wdr36^{+/-}$ and wild-type genotype (Fig. 1C). Subsequently, we took

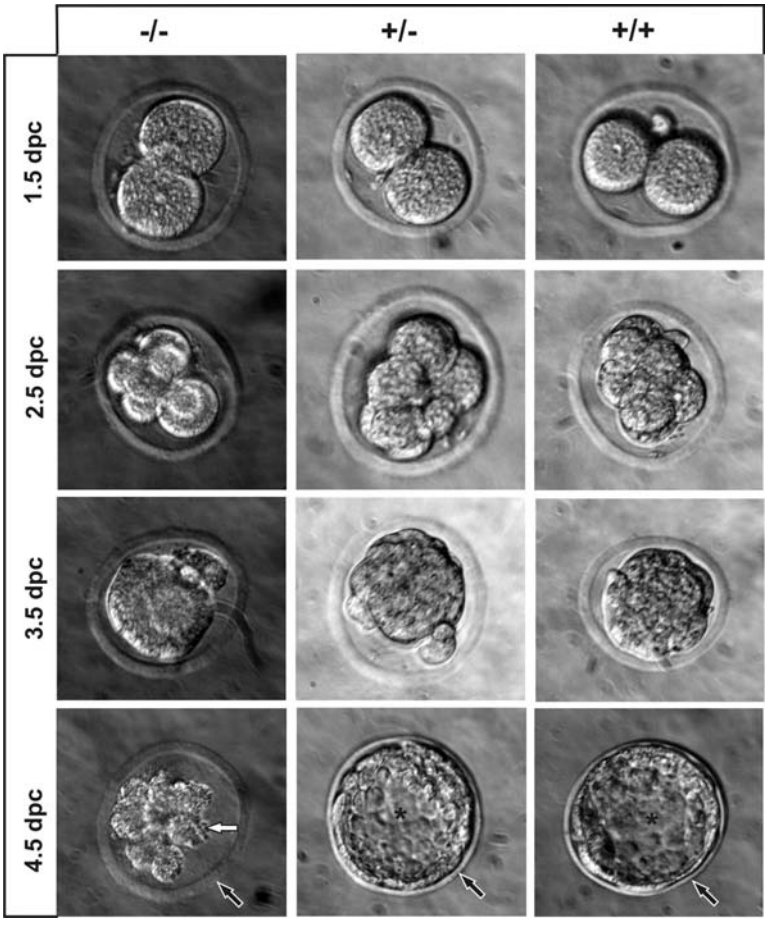

Figure 2. Phenotype of *Wdr36*-deficient embryos. Zygotes were obtained following mating of heterozygous *Wdr36*-deficient animals and kept in KSOM medium at 37°C in humidified air containing 5% CO_2. The same embryos were photographed at 1.5, 2.5, 3.5 and 4.5 dpc. Wild-type and heterozygous *Wdr36*-deficient embryos developed normally and reached blastocyst stage at 4.5 dpc. In contrast, homozygous *Wdr36*-deficient embryos did not reach blastocyst stage and degenerated at 4.5 dpc. Black arrows indicate the zona pellucida which is in contact with embryonic cells surrounding the blastocoel or inner cavity (asterisks) of blastocysts in wild-type and heterozygous *Wdr36*-deficient embryos. In the homozygous *Wdr36*-deficient embryo, the cells have become detached from the zona pellucida and clump together in a cluster (white arrow).

zygotes into culture and observed their development to blastocyst stage. Out of 66 zygotes that were cultured, 15 did not reach blastocyst stage, but instead ceased to develop and degenerated 3.5 days *post coitum* (dpc). In degenerating embryos, the inner cavity or blastocoel of blastocysts did not form and the embryonic cells became detached from their zona pellucida to clump together to a cluster. PCR analysis confirmed that all of those 15 embryos were homozygous *Wdr36* deficient (Fig. 2). Among the 51 embryos that reached blastocyst stage, 17 blastocysts were found to be of wild-type genotype, while 34 were heterozygous *Wdr36* deficient (Fig. 2). Overall, the analysis of cultured embryos confirmed that the loss of *Wdr36* is lethal during preimplantation stages of embryonic development, and pointed towards a Mendelian inheritance of the mutant *Wdr36* locus.

Deficiency in WDR36 leads to apoptotic cell death

Since *Wdr36*-deficient embryos degenerate during preimplantation stages, we hypothesized that the lack of WDR36 causes apoptotic death of blastomeres. To test this hypothesis, we wanted to investigate the effects of WDR36 deficiency in a cell culture model by using RNA interference. We first analyzed by real-time RT–PCR several primary and immortalized human cell lines with regard to their endogenous WDR36 expression, and observed a relative high expression in both primary human trabecular meshwork (HTM) cells and in cells of an immortalized cell line (HTM-N) derived from HTM (Fig. 3). In contrast, the expression of WDR36 was considerably weaker in primary human optic nerve astrocytes, primary human retinal pigmented epithelial cells, primary human retinal microvascular endothelial cells and in HeLa cells (Fig. 3).

Next, we generated two independent siRNA (siRNA 1 and siRNA 2) species to knockdown the expression of WDR36 mRNA in HTM-N cells. After repeated transfection of specific siRNA for three consecutive times, we were able to significantly ($P < 0.05$) decrease the amounts of WDR36 mRNA in HTM-N cells to $23.5 \pm 0.6\%$ (siRNA 1) or $45.5 \pm 9.9\%$ (siRNA 2) when compared with control (lipofectamine treated) cells, an effect that was not seen when non-target siRNA was transfected (Fig. 4A). The siRNA-induced

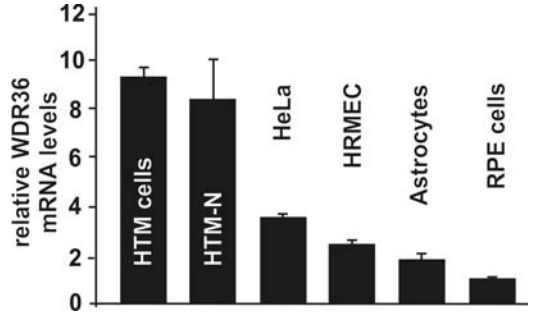

Figure 3. WDR36 expression in human cells *in vitro*. The amounts of WDR36 mRNA in RNA from primary HTM cells, SV40-transformed HTM cells (HTM-N), HeLa cells, human retinal microvascular endothelial cells (HRMEC), human optic nerve astrocytes and human retinal pigmented epithelium (RPE) cells were measured by quantitative real-time RT–PCR. The mean value obtained from mRNA of RPE cells was set as 1. GNB2L was used as a reference gene.

knockdown of WDR36 mRNA resulted in a significantly ($P < 0.05$) smaller number of HTM-N cells in treated culture dishes, while the number of cells in dishes treated with non-target siRNA was not different from that of control dishes (Fig. 4B).

To analyze whether the reduction in cell number was due to an increase in apoptotic cell death, we next determined the relative amounts of cytoplasmic histone-associated DNA fragments (mono- and oligonucleosomes) by ELISA. Significantly ($P < 0.05$ for siRNA 1 and $P < 0.01$ for siRNA 2) higher amounts of cytoplasmic nucleosomes were observed in WDR36-depleted cells following treatment with both species of WDR36 siRNA when compared with controls, while no difference was observed when control cultures were compared with those treated with non-target siRNA (Fig. 4C). Subsequently, we investigated the relative mRNA amounts of genes that are typically upregulated during apoptotic cell death. By real-time RT–PCR, we observed a highly significant ($P < 0.01$) upregulation of BAX (BCL2-associated X protein), an apoptotic activator and member of the BCL2 protein family, in cells treated with WDR36 siRNA when compared with control cells (Fig. 4D). In contrast, the amounts of BAX mRNA in cells treated with non-target siRNA were not significantly different from that of controls. Since the expression of BAX is regulated by the tumor suppressor TP53 (tumor protein 53, p53) and has been shown to be involved in TP53-mediated apoptosis, we next analyzed the expression of TP53 mRNA, which was also found to be significantly higher expressed in cells treated with WDR36 siRNA ($P < 0.05$, Fig. 4E). In contrast, treatment with non-target siRNA decreased the expression of TP53 when compared with controls. TP53 is known to upregulate the expression of CDKN1A (cyclin-dependent kinase inhibitor 1A, p21, Cip1), a molecule that is involved in caspase-mediated apoptosis. By real-time RT–PCR, we observed significantly higher amounts of mRNA for CDKN1A in cell cultures transfected with siRNA 1 than in controls or in cells treated with non-target siRNA ($P < 0.01$, Fig. 4F).

To analyze the possibility that an arrest in cell cycle contributed to the reduced number of cells, which was observed in HTM-N cells following WDR36 knockdown, we performed flow cytometry analyses for DNA content. No obvious differences regarding the number of cells in G1 or G2 stages were observed when comparing cells from cultures treated with siRNA specific for WDR36, non-target siRNA or lipofectamine-treated controls (Fig. 5).

Since our *in vitro* data strongly indicated that the knockdown of WDR36 mRNA causes apoptotic cell death, we finally investigated whether a similar knockdown would have comparable effects *in situ*. To this end, we generated siRNA specific against mouse WDR36 mRNA and injected it into the cytoplasm or into pronuclei of 0.5 dpc mouse zygotes. Most of the WDR36 siRNA- or non-target siRNA-injected zygotes developed a compacted morula (Fig. 6, Table 1). Still, in the WDR36 siRNA group, only a minor percentage (4 out of 36 following cytoplasmic injection and 2 out of 16 following pronucleus injection) developed further to blastocyst stage, while the rest degenerated (Fig. 6, Table 1). In degenerating embryos, the blastocoel did not form and embryonic cells detached from their zona pellucida to clump together to a cluster. In contrast, in the non-target siRNA group, only a minor percentage (3 out of 34 following cytoplasmic injection and 2 out of 18 following pronucleus injection) was found to be degenerated at 4.5 dpc, while the rest had developed to blastocyst stage (Fig. 6, Table 1).

In summary, the knockdown of WDR36 mRNA by RNA interference induced cell death both in cultured cells and in embryos, and the time course of embryonic degeneration following knockdown was similar to that observed in homozygous WDR36-deficient embryos.

WDR36 is localized in the nucleolus of mammalian cells

In a recent study, Skarie *et al*. (41) reported on sequence homologies between WDR36 and Utp21, a nucleolar protein in yeast. They also showed that epitope-tagged recombinant Wdr36 localizes to nucleolus and cytoplasm of zebrafish embryos. To shed light on the subcellular localization of WDR36 in mammalian cells, we performed double-labeling immunocytochemistry with antibodies against WDR36 and B23 (nucleophosmin, a nucleolar phosphoprotein involved in ribosome assembly and transport). In HTM-N cells, staining for both WDR36 and B23 overlapped and was specifically seen in nucleoli (Fig. 7A). In parallel experiments, double-labeling was investigated for WDR36 and PWP2 (periodic tryptophan protein homolog), another nucleolar protein involved in ribosome biogenesis and part of the SSU processome. Confocal microscopy showed that immunoreactivity for both proteins was clearly confined to nucleoli and overlapped in the same nucleolar compartment (Fig. 7B). In addition, immunoreactivity for WDR36 was in the immediate vicinity of the nucleus. In an independent approach, we overexpressed recombinant and epitope-tagged WDR36 in HTM-N cells. Immunocytochemistry with antibodies against the myc-tag predominantly visualized strong immunoreactivity in nucleoli of cells (Fig. 7C). In contrast to the findings for wild-type WDR36, some faint immunoreactivity against the myc-tag of recombinant WDR36 was also seen dispersed throughout the cytoplasm of HTM-N cells. Overall, our immunocytochemical data strongly indicated that WDR36 is a nucleolar protein in mammalian cells.

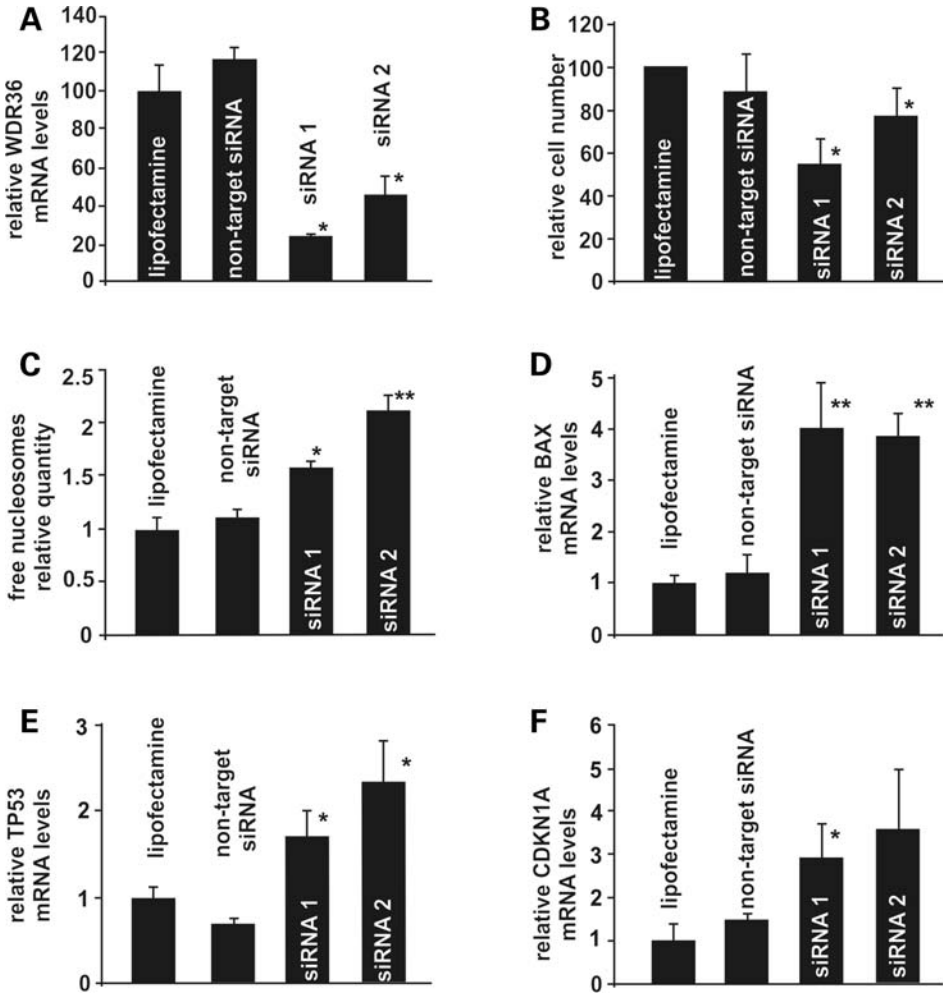

Figure 4. Depletion of WDR36 mRNA in HTM-N cells by RNA interference. (**A**) Real-time RT–PCR analysis for WDR36 mRNA in RNA from HTM-N cells after treatment with lipofectamine, non-target or specific WDR36 siRNAs (siRNA 1 and 2). The mean value obtained with RNA from lipofectamine-treated cells was set at 100%. GNB2L served as a reference gene. (**B**) Relative number of HTM-N cells after treatment with lipofectamine, non-target or specific WDR36 siRNAs (siRNA 1 and 2). The mean value obtained with lipofectamine-treated cells was set at 100%. (**C**) Relative quantity of free nucleosomes as measure of apoptosis in HTM-N cells treated with lipofectamine, non-target or specific WDR36 siRNAs (siRNA 1 and 2). The mean value of lipofectamine-treated cells was set at 1. (**D**–**E**) Real-time RT–PCR analysis for mRNA of BAX (D), TP53 (E) and CDKN1A (**F**) in RNA of HTM-N cells treated with lipofectamine, non-target or specific WDR36 siRNAs (siRNA 1 and 2). The mean value of lipofectamine-treated cells was set at 1. GNB2L was used as a reference gene. Asterisks mark statistically significant differences between lipofectamine-treated and siRNA-treated cells ($*P < 0.05$; $**P < 0.01$).

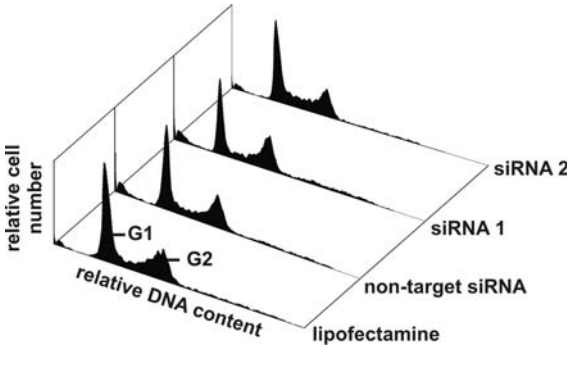

Figure 5. Effects of WDR36 depletion on cell cycle of HTM-N cells. Cells were treated with lipofectamine, non-target or specific WDR36 siRNAs (siRNA 1 and 2) and analyzed on a flow cytometer. G1, cells in G1 phase; G2, cells with replicated DNA in the G2 phase.

WDR36 functions in ribosome biogenesis

Utp21, the putative homolog of WDR36 in yeast, is a component of the SSU processome, a large ribonucleoprotein complex required for the biogenesis of 18S rRNA. The SSU processome participates in a series of events in which primary 47S/45S pre-rRNA is cleaved to yield 18S rRNA, a process that involves two alternative pathways and various intermediate pre-rRNAs in human cells (Fig. 8). 47S/45S pre-rRNA contains, in addition to 18S rRNA, 5.8S rRNA and 28S rRNA, internal transcribed spacers (ITS-1 and ITS-2) and is flanked by external transcribed spacers (ETS). Since ITS1 is removed during the last cleavage steps from 18S precursor rRNA, we hypothesized that by using a probe against ITS-1 we should be able to examine the pre-rRNA maturation process and to visualize if the knockdown of

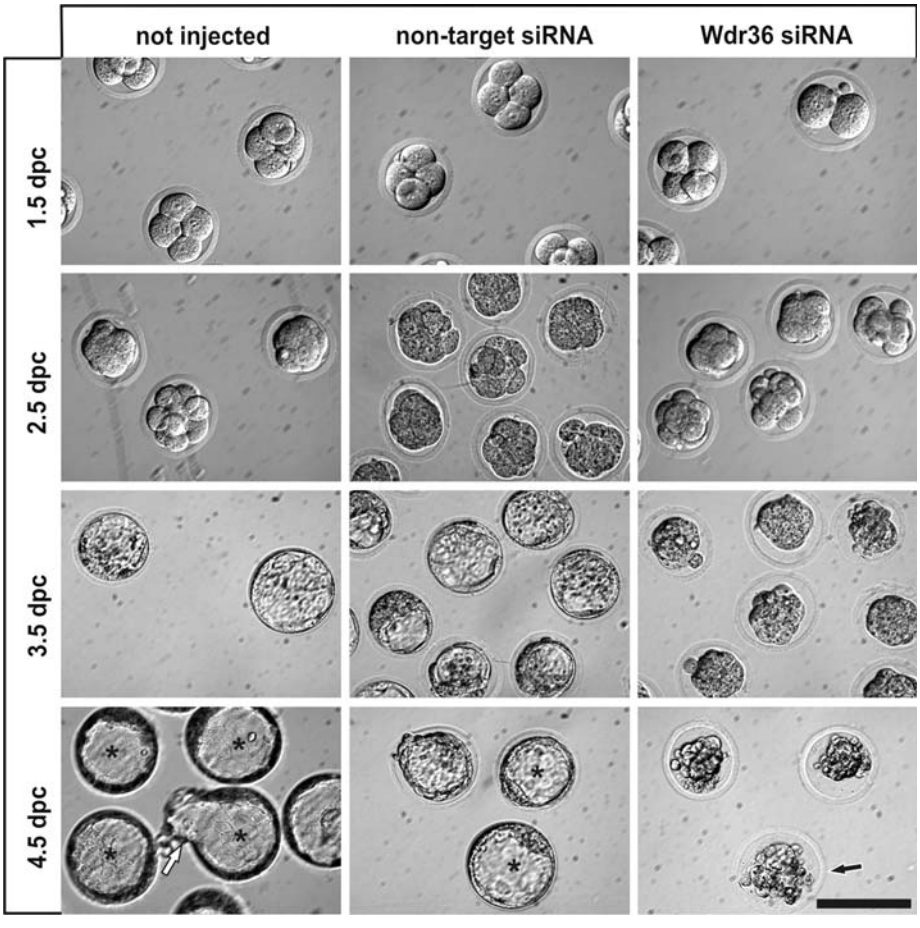

Figure 6. Phenotype of embryos treated with siRNA. siRNA was injected into the cytoplasm or one of the pronuclei, and zygotes were kept in KSOM medium at 37°C in humidified air containing 5% CO_2. The same cultures were photographed at 1.5, 2.5, 3.5 and 4.5 dpc. Non-injected or embryos injected with non-target siRNA develop to blastocysts with a typical inner cavity or blastcoel (asterisks). Some of the embryos are already seen to hatch from their zona pellucida (white arrow). In contrast, embryos injected with WDR36 siRNA do not reach blastocyst stage and degenerate at 4.5 dpc. The black arrow indicates the zona pellucida from which the cells have become detached to clump together in a cluster (white arrow).

WDR36 mRNA leads to a reduced synthesis of intermediate pre-rRNAs of the 18S rRNA pathway.

As expected, the ITS-1 probe hybridized with 47S/45S, 41S, 30S and 21S pre-RNAs which all contain ITS-1, but not with mature 18S rRNA (Fig. 9). In addition, the ITS-1 probe hybridized with a band which migrated very close to that of large subunit 28S rRNA, an observation which we attributed to sequence homologies between ITS-1 and sequences within 28S rRNA, and the extreme high copy number of 28S rRNA. An alternative explanation is the detection of an additional 26S pre-rRNA band resulting from processing of 30S pre-rRNA in the 5′-ETS region as described previously (42). Most noteworthy, a substantial decrease in the amounts of 21S pre-rRNA, the direct precursor of 18S rRNA, was observed following knockdown of WDR36 mRNA when compared with controls (lipofectamine-treated cells) or cells transfected with non-target siRNA (Fig. 9). We next examined pre-rRNA processing in HTM-N cells depleted of WDR36 by pulse-chase labeling with L-[methyl-^{3}H]methionine, which served as a methyl group donor for methylation of pre-rRNAs. Cells were labeled for 30 min, and chase with cold methionine was performed for up to 60 min. HTM-N cells treated with WDR36 siRNA 1 and 2 displayed a different processing pattern when compared with control cells as the formation of 18S rRNA was substantially delayed after a 30 min chase (Fig. 10). In parallel, there was a build-up of the amounts of 47S/45S pre-rRNA and an increase in the ratio of newly produced 28S rRNA versus 18S rRNA following a 60 min chase (Fig. 10). In both northern blot (Fig. 9) and pulse-chase experiments (Fig. 10), small differences regarding the amounts of pre-rRNA were observed between the two controls, e.g. lipofectamine-treated cells or cells transfected with non-target siRNA. Such differences were regarded as not relevant and due to minor differences in loading.

In summary, both northern blot and pulse-chase-labeling experiments provided evidence for a delay in the maturation of 18S rRNA following WDR36 depletion, and for a role of WDR36 in the formation of SSU rRNA in mammalian cells.

DISCUSSION

We conclude that WDR36 is an essential nucleolar protein in mammalian cells which is involved in the processing of SSU 18S rRNA. This conclusion rests upon (i) the observation that homozygous

Table 1. Embryonic development *in vitro* following siRNA injection

0.5 dpc								
Treatment	Zygote	2 cells	4 cells	8 cells	16–32 cells	Morula, compacted	Blastocyst	Blastocyst, hatched
A	17							
B	39							
C	40							
D	16							
E	18							
1.5 dpc								
Treatment	Degenerated/dead	2 cells	4 cells	8 cells	16–32 cells	Morula, compacted	Blastocyst	Blastocyst, hatched
A		14	3					
B	3[a]	32	4					
C	6[a]	34						
D		15	1					
E		17	1					
3.5 dpc								
Treatment	Degenerated/dead	2 cells	4 cells	8 cells	16–32 cells	Morula, compacted	Blastocyst	Blastocyst, hatched
A						10	7	
B						30 + 6[b]		
C					4	21	9	
D						16		
E						13	5	
4.5 dpc								
Treatment	Degenerated/dead	2 cells	4 cells	8 cells	16–32 cells	Morula, compacted	Blastocyst	Blastocyst, hatched
A							2	14
B	32						4	
C	3						5	26
D	14						2	
E	2							16

A, control, no injection; B, injection of WDR36 siRNA into cytoplasm; C, injection of non-target RNA into cytoplasm; D, injection of WDR36 siRNA into pronucleus; E, injection of non-target RNA into pronucleus.
[a]Injection damage.
[b]Partially disintegrated.

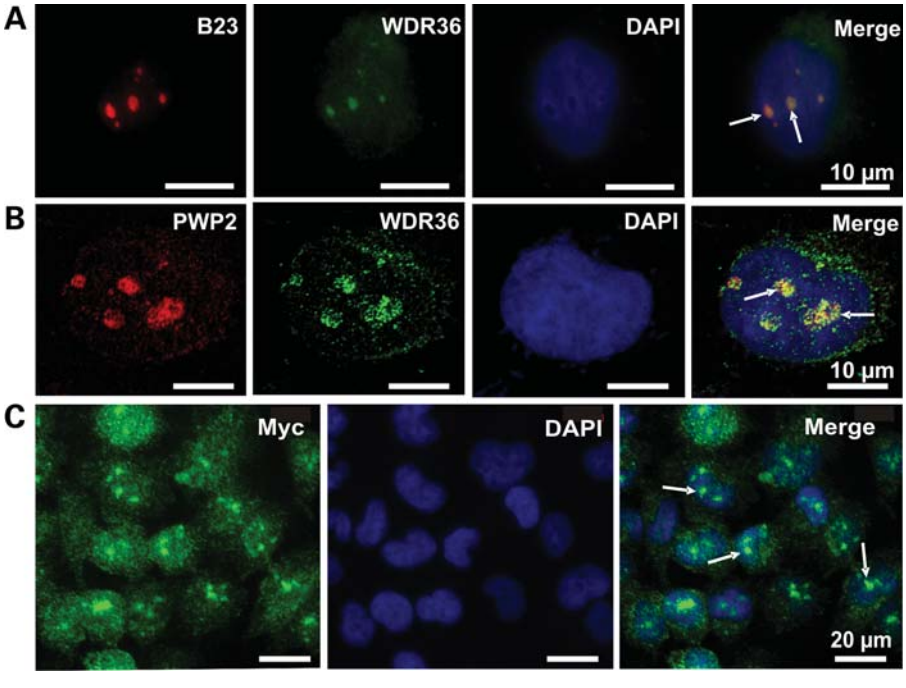

Figure 7. Subcellular localization of WDR36 in HTM-N cells. (**A** and **B**) WDR36 (green) co-localizes with B23 (A, red, fluorescent microscopy) or PWP2 (B, red, confocal microscopy). B23 serves as a nucleolar marker, while PWP2 is a nucleolar protein involved in ribosome biogenesis and part of the SSU processome. (**C**) Recombinant WDR36 containing an Myc-Tag localizes to the nucleolus of HTM-N cells. In addition, cytoplasmic staining is observed. Nuclei are labeled with DAPI (blue).

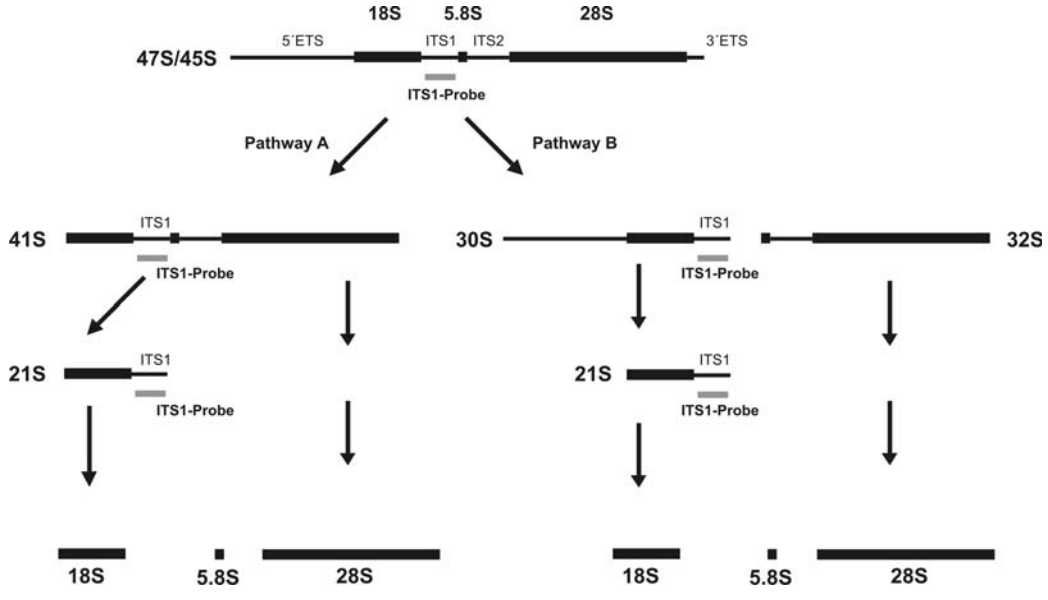

Figure 8. Schematic of pre-rRNA processing in human cells [adapted from (82) and (42)].

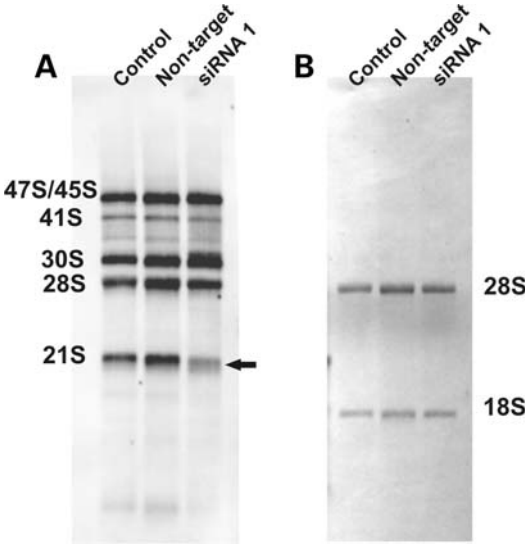

Figure 9. The amounts of 21S pre-rRNA decrease following WDR36 depletion. (**A**) Northern blot analysis of rRNA in RNA from HTM-N cells after treatment with lipofectamine (control), non-target or specific WDR36 siRNAs (siRNA 1). The arrow marks the 21S band in siRNA 1-treated cells. (**B**) Methylene blue staining served as a control for equal loading.

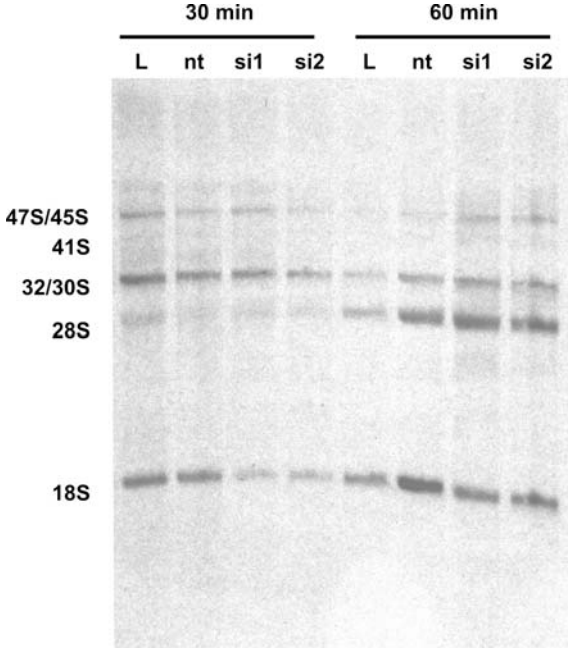

Figure 10. The formation of 18S rRNA is delayed following WDR36 depletion. Pulse-chase analysis of rRNA synthesis with L-[methyl-^{3}H]methionine. HTM-N cells were treated with lipofectamine (l), non-target (nt) or specific WDR36 siRNAs (si1 and si2).

WDR36-deficient embryos degenerate before reaching blastocyst stage, (ii) the findings that depletion of WDR36 mRNA by RNA interference results in both apoptosis of HTM cells and degeneration of preimplantation mouse embryos, (iii) the nucleolar localization of both wild-type and epitope-tagged recombinant WDR36 and finally (iv) the observation that the depletion of WDR36 mRNA results in the delay of 18S rRNA maturation.

Wdr36 is an essential nucleolar protein

During mammalian development, maternally derived mRNAs direct only the first few cleavage divisions. In a process termed maternal-to-zygotic transition (MZT), maternal RNAs and proteins are eliminated, and zygotic transcription is initiated (43,44). In the mouse embryos, zygotic transcription is activated at the two-cell stage and a large fraction of maternally supplied mRNAs, rRNAs and ribosomes is degraded during this stage (45–48). Comparable changes are observed regarding the nucleolus, the site of ribosome-subunit biogenesis in eukaryotic cells (49). The maternally derived nucleoli of the two pronuclei disassemble after pronuclear fusion (50), while zygotic transcription of ribosomal RNA initiates at the

two-cell stage in nucleolar precursor bodies and the nucleoplasm (51–53). Nucleolar precursor bodies are detected throughout the morula state and finally develop into typical nucleoli with their characteristic tripartite morphology (54–57).

It is not surprising though that mouse embryos with a targeted null mutation in genes that encode for proteins critically involved in ribosomal RNA synthesis or processing in the nucleolus such as RBM19 (58), pescadillo-1 (59), fibrillarin (60), RPO1–2 (61), RPS19 (62) or SURF6 (63) typically fail to develop beyond the morula stage. The nucleolar localization of WDR36 along with the observation that homozygous *Wdr36*-deficient embryos degenerate before reaching blastocyst stage strongly indicates an important role for WDR36 in the processing of ribosomal RNA in the nucleolus. Similar to the results of Skarie and Link (41) in zebrafish embryos, we observed that an epitope-tagged recombinant WDR36 localizes to the nucleolus of HTM-N cells, but does also show a cytoplasmic localization. We regard the cytoplasmic localization of recombinant WDR36 as an unspecific consequence of overexpression, since we observed a more specific nucleolar labeling of wild-type WDR36 by immunocytochemistry of HTM-N cells, along with co-staining of typical nucleolar proteins such as B23/nucleophosmin or PWP2. Findings reported following mass spectrometry analysis of nucleoli isolated from human cells support our findings, as WDR36 was found to be a component (http://www.lamondlab.com/NOPdb/) (64).

A characteristic finding which was reported for mouse embryos that are deficient in nucleolar proteins is an increase in apoptosis (58,60,61), a scenario that we also observed when WDR36 was depleted in HTM-N cells and which may well account for degeneration of WDR36-deficient embryos. Apoptosis following depletion of Wdr36 mRNA in zebrafish by viral insertion in the *wdr36* gene or by morpholino anti-sense probes was also reported by Skarie and Link (41). Noteworthy, the depletion of Wdr36 in zebrafish embryos did not cause degeneration of embryos during early developmental stages as observed here in the mouse. In contrast, zebrafish embryos developed well past the onset of organogenesis, although substantial developmental defects were observed in the head, gut and eye formation. Comparable differences regarding the phenotype of mouse and zebrafish embryos that are deficient in the respective homologous protein were also reported for other nucleolar proteins such as RBM19 (65), pescadillo-1 (66) and Rps19 (67,68). A likely explanation for these differences is the fact that, in zebrafish, MZT and zygotic gene activation occur considerably later than during mammalian development, while maternal factors continue to perform essential functions well after MZT (69). Alternatively, viral insertion or treatment with morpholino anti-sense probes very likely does not lead to a complete depletion of Wdr36 mRNA and some residual protein may still be translated, a scenario quite unlike to the situation in a mouse embryo after a targeted disruption of *Wdr36*.

WDR36 and the SSU processome

Maturation of 18S rRNA requires the removal of externally and internally transcribed spacers, a process that is mediated by the SSU processome, which is a large ribonucleoprotein complex containing >40 proteins (70). The SSU processome was discovered in yeast and most of our information concerning it has been obtained from studies in this organism, although some data are available on its role in human cells (71,72). In yeast, the SSU processome consists of several subcomplexes such as the bUTP complex which contains Utp21, the yeast homolog of WDR36. Our data show that the depletion of WDR36 delays the maturation of 18S rRNA, indicating that the functions of WDR36 and Utp21 are similar and conserved from yeast to mammals. The observation that the maturation of 18S rRNA was retarded, but not disrupted, appears to indicate that the depletion of WDR36 was not complete following the knockdown of its mRNA by RNA interference. The reduced amounts of WDR36 very likely slowed down the activity of the SSU processome, but did not completely block it.

WDR36 and its role in diseases

In recent years, a growing number of rare, inherited diseases have been identified, which are caused by mutations in genes that are involved in the biogenesis of the SSU processome or that of small nucleolar ribonucleoproteins or ribosomal proteins (73). For almost all of the encoded proteins, the homolog in yeast is essential. In addition, several of the proteins have been shown to be essential for the mammalian organism. Nearly all of the diseases that are caused by genetic failures in ribosomal processing or synthesis result from haploinsufficiency which leads to the activation of apoptosis via the p53 pathway in distinct, yet different, types of tissues. It appears, therefore, reasonable to assume that haploinsufficiency is the mechanism which accounts for the onset of POAG in patients with mutations in *WDR36*. Apoptotic death of RGC is the cause of vision loss in POAG (74,75) and mutations in *WDR36* might confer a higher vulnerability to stimuli driving RGC towards apoptosis such as an increase in IOP. On the other hand, dominant negative effects may be involved in the role of *WDR36* in POAG, as transgenic mice that overexpress mutant forms of WDR36 under control of a constitutive ubiquitous promoter develop retinal degenerations and show abnormalities in axonal outgrowth (76). Clearly, heterozygous *Wdr36*-deficient mice are an attractive tool to study the effects of haploinsufficiency on RGC in the mouse eye, and such studies are already underway in our laboratory.

MATERIALS AND METHODS

Targeting construct and generation of *Wdr36*-deficient mice

The genomic sequence of the *Wdr36* locus of 129/Ola mice was obtained by PCR. A 2.0 kb fragment immediately upstream of the translation start was obtained by PCR and used as 5′-homology region (Supplementary Material, Table S1). The start codon of *lacZ* was placed exactly over the start codon. A 4.2 kb fragment starting 19.3 kb downstream of the open-reading frame was obtained by PCR and used as 3′-homology region (Supplementary Material, Table S1). The plasmid pTVflox–Wdr36–KO

(Supplementary Material, Fig. S1) was linearized at a unique *Not*I site and electroporated into R1 embryonic stem (ES) cells (129 X1 × 129 S1), which were then selected with G418 (200 μg/ml) and ganciclovir (2 μM). Homologous recombination resulted in the deletion of the start ATG and the first 16 exons. The deleted genomic region was replaced with a *lacZ*-floxed pgk-neomycin cassette. For negative selection, an hsv-tk cassette was placed outside the 5′-homology region. Genotyping was performed by Southern hybridization of ES cell DNA using nonradioactive-labeled DIG probes according to the manufacturer's instructions (DIG Application Manual for Filter Hybridization, Roche Applied Science, Mannheim, Germany). ES cell clones were screened by Southern blotting with a 704 bp 5' probe which recognized a 9042 bp fragment of the wild-type allele and a 4890 bp fragment of the targeted allele in genomic DNA digested with *Eco*RV. An appropriate integration of the 3′ end of the targeting construct was verified by using a 493 bp 3′ probe on ES cell DNA double-digested with *Nco*I and *Xho*I. The probe hybridized to a 5280 bp fragment in the targeted allele, as opposed to a 6142 bp fragment in the wild-type allele. The targeted ES cells were injected into C57BL/6J blastocysts to generate chimeras. Chimeric males transmitted the targeted allele to their offspring. Genotyping was routinely performed by PCR analysis, using a common upper primer located in the 5′ flank upstream of the start codon (5′-GACCTCCCTGAA AATGAGTCAC-3′) and two lower primers located in intron 1 of *Wdr36* (5′-GGATAGCGAGCAAATATGAAGG-3′) and *lacZ* (5′-AATGGGATAGGTTACGTTGGTG-3′) resulting in a 896 bp PCR fragment for the wild-type allele and a 585 bp fragment for the targeted allele. DNA was obtained from tail tips, or in the case of embryos, from yolk sacs (Reichert's membrane). PCR was performed in 25 μl reaction mixtures containing standard buffer, 0.1 μM of each primer, 1 mM dNTPs, 2.5 mM $MgCl_2$, 12% glycerol, 0.2 mM cresol red sodium salt (Sigma, Taufkirchen, Germany) and 0.25 U *Taq*-Polymerase (New England Biolabs, Frankfurt am Main, Germany). The cycling conditions consisted of an initial 2 min denaturing step at 94°C, followed by 35 cycles for 20 s at 94°C, for 20 s at 58°C, for 45 s at 72°C. Mice were housed at a 12 h light/dark cycle under standardized conditions of 62% air humidity and 21°C room temperature (RT).

Preimplantation stage embryos

For timed pregnancies, $Wdr36^{+/-}$ females received an i.p. injection of serum gonadotropin from a pregnant mare (5 IU/animal; Sigma), followed 48 h later by human chorionic gonadotropin (5 IU/animal; Sigma). Mice were then allowed to mate with $Wdr36^{+/-}$ males. The males were removed the next morning and the females were examined for the presence of a vaginal plug. Preimplantation stage embryos (zygotes at 0.5 dpc, and blastocysts at 3.5 dpc) were collected by flushing the uterus of plugged females with M2 medium (Sigma). Flushed embryos were cultured individually in KSOM (Millipore, Billerica, USA) microdrop cultures at 37°C in humidified air containing 5% CO_2 over several days. The growth patterns of embryos were microscopically examined and photographed. DNA was prepared by incubation of individual embryos with 20 μl of lysis buffer [50 mM Tris–HCl, 0.5% Triton X-100, proteinase K (500 μg/ml), pH 8.0] for 4 h at 55°C, followed by incubation at 90°C for 10 min. Two microliters of embryonic DNA were used in the first round of a nested PCR strategy. First-round primers were identical to that used for genotyping of litters. For the second round of amplification, 1 μl of the first-round reaction mixture was added to two separate reaction mixtures, each containing the internal forward wild-type primer (5′-CAACCAAGAGGA AACCAACC-3′) and an internal reverse wild-type primer (5′-CTAAGTGCAAGGGCACAAGG-3′) or an internal reverse *lacZ* primer (5′-GGCGATTAAGTTGGGTAACG-3′). PCR conditions were identical to that described above. Microinjection was performed under an inverted microscope (Olympus IX71) at 320-fold magnification with differential interference contrast (DIC) using electromechanical micromanipulators (Eppendorf TransferMan NK2). Twenty micromolars of siRNA were injected into the cytoplasm (10–20 pl) or one of the pronuclei (2–4 pl) of zygotes with fine-drawn glass capillaries of a 0.5–2 μm opening diameter under a constant pressure of 10–50 hPa depending on the opening size. The pressure was produced and regulated by a FemtoJet compressor (Eppendorf). All injected embryos were allowed to develop to the blastocyst stage in culture. The growth patterns of embryos were microscopically examined and photographed.

Cell culture

Primary HTM cells, human optic nerve astrocytes, human retinal pigmented epithelium cells, human retinal microvascular cells and immortalized simian virus 40 (SV40) transformed HTM cells (HTM-N) were cultured as described previously (77–81). To generate a cell line with stable overexpression of WDR36, the full-length cDNA of mouse WDR36 was cloned and ligated into plasmid pCDNA3.1A (Invitrogen, Karlsruhe, Germany) to allow expression of WDR36 with both a C-terminal c-myc epitope and a 6x His tag under control of the cytomegalovirus promoter. HTM-N cells transfected with plasmid mmWdr36–pcDNA.3.1/*myc*–His were cultured in the presence of 1% G418 (PAA, Pasching, Austria). For transfection, lipofectamine 2000 was used according to manufacturer's instructions (Invitrogen). The number of cultured cells was assessed by automated counting (CASY Cell Counter and Analyser TT, Schärfer, Reutlingen, Germany). For analyzing cell-cycle profiles, cells were fixed with 70% ethanol overnight at −20°C, incubated with 100 mg/ml of RNase A for 60 min at 37°C followed by 50 μg/ml of propidium iodide for 30 min. Data were acquired on a flow cytometer (Partec CA-III, Münster, Germany) and analyzed using WinMDI 2.8 software (J. Trotter, The Scripps Institute, Flow Cytometry Core Facility). Cell death detection ELISA (Roche) was performed according to the manufacturer's instructions.

Generation and transfection of siRNA

Target sequences for mouse and human WDR36 siRNA were designed according to the Ambion web-based criteria and generated with a Silencer siRNA construction kit (Ambion, Austin, TX, USA). Different WDR36 siRNAs were tested in initial transfection experiments and subsequent RT–PCR

Table 2. Primers used for real-time RT–PCR

BAX fwd	5′-ATGTTTTCTGACGGCAACTTC-3′
BAX rev	5′-ATCAGTTCCGGCACCTTG-3′
GNB2L fwd	5′-GCTACTACCCCGCAGTTCC-3′
GNB2L rev	5′-CAGTTTCCACATGATGATGGTC-3′
CDKN1A fwd	5′-TCACTGTCTTGTACCCTTGTGC-3′
CDKN1A rev	5′-GGCGTTTGGAGTGGTAGAAA-3′
TP53 fwd	5′-AGGCCTTGGAACTCAAGGAT-3′
TP53 rev	5′-CCCTTTTTGGACTTCAGGTG-3′
WDR36 fwd	5′-AGTTTTGGCAAGGATCAAGC-3′
WDR36 rev	5′-TCCAGAATTTGAGTAATCCTTCACT-3′

analysis. Best results were obtained by transfecting 50 nM of the WDR36 siRNA 1 and WDR36 siRNA 2 using lipofectamine 2000 for transfection. The primers used to generate human WDR36 siRNA 1 were 5′-AAGCGCCGGTTCTATG TAACACCTGTCTC-3′ (sense) and 5′-AATGTTACATAG AACCGGCGCCCTGTCTC-3′ (antisense). For generation of human WDR36 siRNA 2, primers 5′-AATTGCCGGACTGA CATTTCTCCTGTCTC-3′ (sense) and 5′-AAAGAAATGT CAGTCCGGCAACCTGTCTC-3′ (antisense) were used. To assess the effects of WDR36 siRNA on gene expression, cells were transfected three times at 24, 48 and 72 h after seeding and supplemented after 4 h with culture medium. After the last transfection, the cells were incubated for 48 h before harvesting. siSTABLE non-targeting siRNA 1 (Dharmacon, Chicago, USA), a chemically modified (for increased stability) control siRNA with at least four mismatches to any human, mouse, or rat gene, was used as a negative control. Primers used for generation of mouse-specific WDR36 siRNA as used in microinjection assays were 5′-AAGCGCCGCTTCTACGTGACGCCTGTCTC-3′ (sense) and 5′-AACGTCACGTAGAAGCGGCGCCCTGTCTC-3′ (antisense).

RNA isolation and analysis

Total RNA was extracted with TRIzol (Invitrogen) according to manufacturer's recommendations. Structural integrity of RNA samples was confirmed by electrophoresis using 1% (w/v) agarose gels. The RNA concentration was determined by absorbance at 260 nm. First-strand cDNA was prepared from total RNA, using the iScript cDNA Synthesis kit (BioRad, München, Germany) according to the manufacturer's instructions. Real-time RT–PCR was performed on a BioRad iQ5 Real-Time PCR Detection System (BioRad) with the temperature profile as follows: 40 cycles for 10 s melting at 95°C, 40 s of annealing and extension at 60°C. Primer pairs (Table 2) were purchased from Invitrogen and extended over exon–intron boundaries. RNA that was not reverse transcribed served as a negative control for real–time PCR. Guanine nucleotide binding protein 2 (GNB2L) served as a housekeeping gene. For northern blot analysis, RNA was size fractionated on a 1% agarose gel containing 3% formaldehyde and blotted onto a positively charged nylon membrane (Roche). After transfer, the blot was cross-linked using an UV Stratalinker 1800 (Stratagene, La Jolla, CA, USA) followed by methylene blue staining (0.03% methylene blue, 0.3 M sodium acetate, pH 5.2) to assess the amount and quality of the RNA. Prehybridization was performed for 45 min at 68°C in a Hybridizer HB-1000 (UVP Laboratory Products, Upland, CA, USA) using the Dig EasyHyb-buffer (Roche). Antisense RNA probes were generated of genomic DNA using ITS-1 fwd (5′-GAGAACTCG GGAGGGAGAC-3′) and ITS-1-T7 rev (5′-TAATACGACT CACTATAGGGAGACGCCCTAGCGGGAAG-3′) primers and labeled using DIG RNA Labeling kit (Roche) according to the manufacturer's instructions. Hybridization was performed for 16–18 h at 68°C. Membranes were washed two times for 5 min with 2× saline-sodium citrate (SSC) and 0.1% sodium dodecyl sulfate (SDS) at RT followed by two washes with 0.2% SSC and 0.1% SDS at 70°C for 15 min. After an additional washing step with maleic acid wash buffer (0.1 M maleic acid, 0.15 M sodium chloride, 0.3% Tween 20, pH 7.5), the membrane was blocked for 30 min in 1× DIG-blocking reagent (Roche) at RT. Then the blot was incubated for 30 min with Anti-DIG-antibody (1:10 000 in 1× DIG-blocking reagent (Roche), washed with maleic acid wash buffer (2 × 15 min, RT) and equilibrated in detection buffer (100 mM Tris–HCl, 100 mM NaCl; pH 9.5) for 10 min. For detection, blots were incubated with chemiluminescence substrate CDP-STAR (Roche) and documented in a LAS 3000 Intelligent Dark box (Fujifilm, Düsseldorf, Germany).

Pulse chase

For pulse-chase experiments, a knockdown of WDR36 was performed in HTM-N cells as described above. Forty-eight hours after the last transfection, cells were washed two times with phosphate-buffered saline (PBS) followed by 30 min incubation with methionine-free medium. Twenty-five microcurie L-[methyl-^{3}H]-methionine was added to the medium, and the cells were incubated for 30 min at 37°C, 7% CO_2. The radioactive medium was replaced by normal growth medium and cells were harvested after 15, 30 and 60 min of chase time.

Immunocytochemistry

HTM-N cells were grown on microscope slides as described above. After incubation, cells were fixed in 4% paraformaldehyde for 15 min, washed twice in 0.1 M PBS, pH 7.2, and subsequently incubated for 5 min in 0.1 M PBS containing 0.5% Triton X-100 followed by two washing steps with 0.1 M PBS. Cells were blocked for 45 min in 3% bovine serum albumin (BSA) and 0.1% Triton X-100 in 0.1 M PBS. Primary antibodies were added in appropriate dilutions [rabbit anti-WDR36 polyclonal (Abcam): 1:50, mouse anti-B23 polyclonal (Abcam): 1:500 and mouse anti-PWP2H polyclonal (Abcam): 1:75] in PBS/BSA (0.3%) and allowed to bind for 2 h at RT. After the cells were washed three times with PBS, secondary antibodies [highly cross adsorbed goat anti-rabbit conjugated to Alexa 488 (Invitrogen); highly cross adsorbed donkey anti-mouse conjugated to Cy3 (Jackson Immuno Research)] were added for 1 h at RT. 4′,6-Diamidino-2-phenylindole (DAPI) was used to counterstain nuclear DNA. Slides were mounted in a medium containing DAPI (Vectashield; Vector Laboratories, Burlington, CA, USA), and analyzed under a fluorescence microscope (Zeiss

Axio Imager; Carl Zeiss AG, Oberkochen, Germany). To control for non-specific binding of secondary antibodies, negative control experiments were performed, which were handled similarly, with the exception that the cells were incubated in PBS/BSA instead of primary antibody.

Statistics

All results are expressed as mean ± SEM. Comparisons between the mean variables of the two groups were made by a two-tailed Student's *t*-test. *P*-values <0.05 were considered to be statistically significant.

SUPPLEMENTARY MATERIAL

Supplementary Material is available at *HMG* online.

Conflict of Interest statement. None declared.

FUNDING

This work was supported by the Deutsche Forschungsgemeinschaft (FOR 1075, TP5 to E.R.T.).

REFERENCES

1. Resnikoff, S., Pascolini, D., Etya'ale, D., Kocur, I., Pararajasegaram, R., Pokharel, G.P. and Mariotti, S.P. (2004) Global data on visual impairment in the year 2002. *Bull. World Health Organ.*, **82**, 844–851.
2. Kwon, Y.H., Fingert, J.H., Kuehn, M.H. and Alward, W.L. (2009) Primary open-angle glaucoma. *N. Engl. J. Med.*, **360**, 1113–1124.
3. Tamm, E.R., Toris, C.B., Crowston, J.G., Sit, A., Lim, S., Lambrou, G. and Alm, A. (2007) Basic science of intraocular pressure. In Weinreb, R.N., Brandt, J.D., Garway-Heath, D. and Medeiros, F. (eds), *Intraocular Pressure. Reports and Consensus Statements of the 4th global AIGS Consensus Meeting on Intraocular Pressure*. Kugler Publications, Amsterdam, pp. 1–14.
4. Johnson, M. (2006) What controls aqueous humour outflow resistance?. *Exp. Eye Res.*, **82**, 545–557.
5. The AGIS Investigators (2000) The advanced glaucoma intervention study (AGIS): 7. The relationship between control of intraocular pressure and visual field deterioration. *Am. J. Ophthalmol.*, **130**, 429–440.
6. Collaborative Normal-Tension Glaucoma Study Group (1998) The effectiveness of intraocular pressure reduction in the treatment of normal-tension glaucoma. Collaborative Normal-Tension Glaucoma Study Group. *Am. J. Ophthalmol.*, **126**, 498–505.
7. Leske, M.C., Heijl, A., Hussein, M., Bengtsson, B., Hyman, L. and Komaroff, E. (2003) Factors for glaucoma progression and the effect of treatment: the early manifest glaucoma trial. *Arch. Ophthalmol.*, **121**, 48–56.
8. Collaborative Normal-Tension Glaucoma Study Group (1998) Comparison of glaucomatous progression between untreated patients with normal-tension glaucoma and patients with therapeutically reduced intraocular pressures. *Am. J. Ophthalmol.*, **126**, 487–497.
9. Higginbotham, E.J., Gordon, M.O., Beiser, J.A., Drake, M.V., Bennett, G.R., Wilson, M.R. and Kass, M.A. (2004) The Ocular Hypertension Treatment Study: topical medication delays or prevents primary open-angle glaucoma in African American individuals. *Arch. Ophthalmol.*, **122**, 813–820.
10. Gordon, M.O., Beiser, J.A., Brandt, J.D., Heuer, D.K., Higginbotham, E.J., Johnson, C.A., Keltner, J.L., Miller, J.P., Parrish, R.K. II, Wilson, M.R. *et al.* (2002) The Ocular Hypertension Treatment Study: baseline factors that predict the onset of primary open-angle glaucoma. *Arch. Ophthalmol.*, **120**, 714–720; discussion, pp. 829–730.
11. Johnson, E.C., Guo, Y., Cepurna, W.O. and Morrison, J.C. (2009) Neurotrophin roles in retinal ganglion cell survival: lessons from rat glaucoma models. *Exp. Eye Res.*, **88**, 808–815.
12. Weber, A.J., Harman, C.D. and Viswanathan, S. (2008) Effects of optic nerve injury, glaucoma, and neuroprotection on the survival, structure, and function of ganglion cells in the mammalian retina. *J. Physiol.*, **586**, 4393–4400.
13. Wiggs, J.L. (2007) Genetic etiologies of glaucoma. *Arch. Ophthalmol.*, **125**, 30–37.
14. Allingham, R.R., Liu, Y. and Rhee, D.J. (2009) The genetics of primary open-angle glaucoma: a review. *Exp. Eye Res.*, **88**, 837–844.
15. Stone, E.M., Fingert, J.H., Alward, W.L.M., Nguyen, T.D., Polansky, J.R., Sunden, S.L.F., Nishimura, D., Clark, A.F., Nystuen, A., Nichols, B.E. *et al.* (1997) Identification of a gene that causes primary open angle glaucoma. *Science*, **275**, 668–670.
16. Rezaie, T., Child, A., Hitchings, R., Brice, G., Miller, L., Coca-Prados, M., Heon, E., Krupin, T., Ritch, R., Kreutzer, D. *et al.* (2002) Adult-onset primary open-angle glaucoma caused by mutations in optineurin. *Science*, **295**, 1077–1079.
17. Monemi, S., Spaeth, G., DaSilva, A., Popinchalk, S., Ilitchev, E., Liebmann, J., Ritch, R., Heon, E., Crick, R.P., Child, A. *et al.* (2005) Identification of a novel adult-onset primary open-angle glaucoma (POAG) gene on 5q22.1. *Hum. Mol. Genet.*, **14**, 725–733.
18. Wiggs, J.L., Allingham, R.R., Vollrath, D., Jones, K.H., De La, P.M., Kern, J., Patterson, K., Babb, V.L., Del Bono, E.A., Broomer, B.W. *et al.* (1998) Prevalence of mutations in TIGR/Myocilin in patients with adult and juvenile primary open-angle glaucoma [letter]. *Am. J. Hum. Genet.*, **63**, 1549–1552.
19. Fingert, J.H., Heon, E., Liebmann, J.M., Yamamoto, T., Craig, J.E., Rait, J., Kawase, K., Hoh, S.T., Buys, Y.M., Dickinson, J. *et al.* (1999) Analysis of myocilin mutations in 1703 glaucoma patients from five different populations. *Hum. Mol. Genet.*, **8**, 899–905.
20. Tamm, E.R. (2002) Myocilin and glaucoma: facts and ideas. *Prog. Retin. Eye Res.*, **21**, 395–428.
21. Resch, Z.T. and Fautsch, M.P. (2009) Glaucoma-associated myocilin: a better understanding but much more to learn. *Exp. Eye Res.*, **88**, 704–712.
22. Tamm, E.R. (2008) The functional role of myocilin in glaucoma. In Shields, M.B., Tombran-Tink, J. and Barnstable, C.J. (eds), *Ophthalmology Research: Mechanisms of the Glaucomas*. Humana Press, Totawa, NJ, pp. 219–231.
23. Sahlender, D.A., Roberts, R.C., Arden, S.D., Spudich, G., Taylor, M.J., Luzio, J.P., Kendrick-Jones, J. and Buss, F. (2005) Optineurin links myosin VI to the Golgi complex and is involved in Golgi organization and exocytosis. *J. Cell. Biol.*, **169**, 285–295.
24. Tamm, E.R. (2009) Molecular approaches to glaucoma: intriguing clues for pathology. In Civan, M.M. (ed.), *Current Topics in Membranes, The Eye's Aqueous Humor*, Vol. 62. Elsevier, Amsterdam, pp. 379–425.
25. Park, B.C., Shen, X., Samaraweera, M. and Yue, B.Y. (2006) Studies of optineurin, a glaucoma gene: Golgi fragmentation and cell death from overexpression of wild-type and mutant optineurin in two ocular cell types. *Am. J. Pathol.*, **169**, 1976–1989.
26. Fingert, J.H., Alward, W.L., Kwon, Y.H., Shankar, S.P., Andorf, J.L., Mackey, D.A., Sheffield, V.C. and Stone, E.M. (2007) No association between variations in the WDR36 gene and primary open-angle glaucoma. *Arch. Ophthalmol.*, **125**, 434–436.
27. Weisschuh, N., Wolf, C., Wissinger, B. and Gramer, E. (2007) Variations in the WDR36 gene in German patients with normal tension glaucoma. *Mol. Vis.*, **13**, 724–729.
28. Hewitt, A.W., Dimasi, D.P., Mackey, D.A. and Craig, J.E. (2006) A glaucoma case-control study of the WDR36 gene D658G sequence variant. *Am. J. Ophthalmol.*, **142**, 324–325.
29. Hauser, M.A., Allingham, R.R., Linkroum, K., Wang, J., LaRocque-Abramson, K., Figueiredo, D., Santiago-Turla, C., del Bono, E.A., Haines, J.L., Pericak-Vance, M.A. *et al.* (2006) Distribution of WDR36 DNA sequence variants in patients with primary open-angle glaucoma. *Invest. Ophthalmol. Vis. Sci.*, **47**, 2542–2546.
30. Pasutto, F., Mardin, C.Y., Michels-Rautenstrauss, K., Weber, B.H., Sticht, H., Chavarria-Soley, G., Rautenstrauss, B., Kruse, F. and Reis, A. (2008) Profiling of WDR36 missense variants in German patients with glaucoma. *Invest. Ophthalmol. Vis. Sci.*, **49**, 270–274.
31. Fan, B.J., Wang, D.Y., Cheng, C.Y., Ko, W.C., Lam, S.C. and Pang, C.P. (2009) Different WDR36 mutation pattern in Chinese patients with primary open-angle glaucoma. *Mol. Vis.*, **15**, 646–653.
32. Miyazawa, A., Fuse, N., Mengkegale, M., Ryu, M., Seimiya, M., Wada, Y. and Nishida, K. (2007) Association between primary open-angle

glaucoma and WDR36 DNA sequence variants in Japanese. *Mol. Vis.*, **13**, 1912–1919.
33. Frezzotti, P., Pescucci, C., Papa, F.T., Iester, M., Mittica, V., Motolese, I., Peruzzi, S., Artuso, R., Longo, I., Mencarelli, M.A. *et al.* (2010) Association between primary open-angle glaucoma (POAG) and WDR36 sequence variance in Italian families affected by POAG. *Br. J. Ophthalmol.* [Epub ahead of print].
34. Gudbjartsson, D.F., Bjornsdottir, U.S., Halapi, E., Helgadottir, A., Sulem, P., Jonsdottir, G.M., Thorleifsson, G., Helgadottir, H., Steinthorsdottir, V., Stefansson, H. *et al.* (2009) Sequence variants affecting eosinophil numbers associate with asthma and myocardial infarction. *Nat. Genet.*, **41**, 342–347.
35. Rothenberg, M.E., Spergel, J.M., Sherrill, J.D., Annaiah, K., Martin, L.J., Cianferoni, A., Gober, L., Kim, C., Glessner, J., Frackelton, E. *et al.* (2010) Common variants at 5q22 associate with pediatric eosinophilic esophagitis. *Nat. Genet.*, **42**, 289–291.
36. Smith, T.F., Gaitatzes, C., Saxena, K. and Neer, E.J. (1999) The WD repeat: a common architecture for diverse functions. *Trends Biochem. Sci.*, **24**, 181–185.
37. Li, D. and Roberts, R. (2001) WD-repeat proteins: structure characteristics, biological function, and their involvement in human diseases. *Cell. Mol. Life Sci.*, **58**, 2085–2097.
38. Footz, T.K., Johnson, J.L., Dubois, S., Boivin, N., Raymond, V. and Walter, M.A. (2009) Glaucoma-associated WDR36 variants encode functional defects in a yeast model system. *Hum. Mol. Genet.*, **18**, 1276–1287.
39. Bernstein, K.A., Gallagher, J.E., Mitchell, B.M., Granneman, S. and Baserga, S.J. (2004) The small-subunit processome is a ribosome assembly intermediate. *Eukaryot. Cell*, **3**, 1619–1626.
40. Kressler, D., Hurt, E. and Bassler, J. (2010) Driving ribosome assembly. *Biochim. Biophys. Acta*, **1803**, 673–683.
41. Skarie, J.M. and Link, B.A. (2008) The primary open-angle glaucoma gene WDR36 functions in ribosomal RNA processing and interacts with the p53 stress-response pathway. *Hum. Mol. Genet.*, **17**, 2474–2485.
42. Rouquette, J., Choesmel, V. and Gleizes, P.E. (2005) Nuclear export and cytoplasmic processing of precursors to the 40S ribosomal subunits in mammalian cells. *EMBO J.*, **24**, 2862–2872.
43. Tadros, W. and Lipshitz, H.D. (2009) The maternal-to-zygotic transition: a play in two acts. *Development*, **136**, 3033–3042.
44. Schier, A.F. (2007) The maternal–zygotic transition: death and birth of RNAs. *Science*, **316**, 406–407.
45. Schultz, R.M. (1993) Regulation of zygotic gene activation in the mouse. *Bioessays*, **15**, 531–538.
46. Paynton, B.V., Rempel, R. and Bachvarova, R. (1988) Changes in state of adenylation and time course of degradation of maternal mRNAs during oocyte maturation and early embryonic development in the mouse. *Dev. Biol.*, **129**, 304–314.
47. Piko, L. and Clegg, K.B. (1982) Quantitative changes in total RNA, total poly(A), and ribosomes in early mouse embryos. *Dev. Biol.*, **89**, 362–378.
48. Schultz, R.M. (2002) The molecular foundations of the maternal to zygotic transition in the preimplantation embryo. *Hum. Reprod. Update*, **8**, 323–331.
49. Boisvert, F.M., van Koningsbruggen, S., Navascues, J. and Lamond, A.I. (2007) The multifunctional nucleolus. *Nat. Rev. Mol. Cell. Biol.*, **8**, 574–585.
50. Ogushi, S., Palmieri, C., Fulka, H., Saitou, M., Miyano, T. and Fulka, J. Jr. (2008) The maternal nucleolus is essential for early embryonic development in mammals. *Science*, **319**, 613–616.
51. Svarcova, O., Dinnyes, A., Polgar, Z., Bodo, S., Adorjan, M., Meng, Q. and Maddox-Hyttel, P. (2009) Nucleolar re-activation is delayed in mouse embryos cloned from two different cell lines. *Mol. Reprod. Dev.*, **76**, 132–141.
52. Romanova, L., Korobova, F., Noniashvilli, E., Dyban, A. and Zatsepina, O. (2006) High resolution mapping of ribosomal DNA in early mouse embryos by fluorescence *in situ* hybridization. *Biol. Reprod.*, **74**, 807–815.
53. Zatsepina, O., Baly, C., Chebrout, M. and Debey, P. (2003) The step-wise assembly of a functional nucleolus in preimplantation mouse embryos involves the cajal (coiled) body. *Dev. Biol.*, **253**, 66–83.
54. Grondahl, C. and Hyttel, P. (1996) Nucleologenesis and ribonucleic acid synthesis in preimplantation equine embryos. *Biol. Reprod.*, **55**, 769–774.
55. Hyttel, P., Viuff, D., Fair, T., Laurincik, J., Thomsen, P.D., Callesen, H., Vos, P.L., Hendriksen, P.J., Dieleman, S.J., Schellander, K. *et al.* (2001) Ribosomal RNA gene expression and chromosome aberrations in bovine oocytes and preimplantation embryos. *Reproduction*, **122**, 21–30.
56. Tesarik, J., Kopecny, V., Plachot, M. and Mandelbaum, J. (1987) High-resolution autoradiographic localization of DNA-containing sites and RNA synthesis in developing nucleoli of human preimplantation embryos: a new concept of embryonic nucleologenesis. *Development*, **101**, 777–791.
57. Viuff, D., Greve, T., Holm, P., Callesen, H., Hyttel, P. and Thomsen, P.D. (2002) Activation of the ribosomal RNA genes late in the third cell cycle of porcine embryos. *Biol. Reprod.*, **66**, 629–634.
58. Zhang, J., Tomasini, A.J. and Mayer, A.N. (2008) RBM19 is essential for preimplantation development in the mouse. *BMC Dev. Biol.*, **8**, 115.
59. Lerch-Gaggl, A., Haque, J., Li, J., Ning, G., Traktman, P. and Duncan, S.A. (2002) Pescadillo is essential for nucleolar assembly, ribosome biogenesis, and mammalian cell proliferation. *J. Biol. Chem.*, **277**, 45347–45355.
60. Newton, K., Petfalski, E., Tollervey, D. and Caceres, J.F. (2003) Fibrillarin is essential for early development and required for accumulation of an intron-encoded small nucleolar RNA in the mouse. *Mol. Cell. Biol.*, **23**, 8519–8527.
61. Chen, H., Li, Z., Haruna, K., Semba, K., Araki, M., Yamamura, K. and Araki, K. (2008) Early pre-implantation lethality in mice carrying truncated mutation in the RNA polymerase 1–2 gene. *Biochem. Biophys. Res. Commun.*, **365**, 636–642.
62. Matsson, H., Davey, E.J., Draptchinskaia, N., Hamaguchi, I., Ooka, A., Leveen, P., Forsberg, E., Karlsson, S. and Dahl, N. (2004) Targeted disruption of the ribosomal protein S19 gene is lethal prior to implantation. *Mol. Cell. Biol.*, **24**, 4032–4037.
63. Romanova, L.G., Anger, M., Zatsepina, O.V. and Schultz, R.M. (2006) Implication of nucleolar protein SURF6 in ribosome biogenesis and preimplantation mouse development. *Biol. Reprod.*, **75**, 690–696.
64. Andersen, J.S., Lyon, C.E., Fox, A.H., Leung, A.K., Lam, Y.W., Steen, H., Mann, M. and Lamond, A.I. (2002) Directed proteomic analysis of the human nucleolus. *Curr. Biol.*, **12**, 1–11.
65. Mayer, A.N. and Fishman, M.C. (2003) Nil per os encodes a conserved RNA recognition motif protein required for morphogenesis and cytodifferentiation of digestive organs in zebrafish. *Development*, **130**, 3917–3928.
66. Allende, M.L., Amsterdam, A., Becker, T., Kawakami, K., Gaiano, N. and Hopkins, N. (1996) Insertional mutagenesis in zebrafish identifies two novel genes, pescadillo and dead eye, essential for embryonic development. *Genes Dev.*, **10**, 3141–3155.
67. Danilova, N., Sakamoto, K.M. and Lin, S. (2008) Ribosomal protein S19 deficiency in zebrafish leads to developmental abnormalities and defective erythropoiesis through activation of p53 protein family. *Blood*, **112**, 5228–5237.
68. Uechi, T., Nakajima, Y., Chakraborty, A., Torihara, H., Higa, S. and Kenmochi, N. (2008) Deficiency of ribosomal protein S19 during early embryogenesis leads to reduction of erythrocytes in a zebrafish model of Diamond-Blackfan anemia. *Hum. Mol. Genet.*, **17**, 3204–3211.
69. Pelegri, F. (2003) Maternal factors in zebrafish development. *Dev. Dyn.*, **228**, 535–554.
70. Henras, A.K., Soudet, J., Gerus, M., Lebaron, S., Caizergues-Ferrer, M., Mougin, A. and Henry, Y. (2008) The post-transcriptional steps of eukaryotic ribosome biogenesis. *Cell. Mol. Life Sci.*, **65**, 2334–2359.
71. Turner, A.J., Knox, A.A., Prieto, J.L., McStay, B. and Watkins, N.J. (2009) A novel small-subunit processome assembly intermediate that contains the U3 snoRNP, nucleolin, RRP5, and DBP4. *Mol. Cell. Biol.*, **29**, 3007–3017.
72. Prieto, J.L. and McStay, B. (2007) Recruitment of factors linking transcription and processing of pre-rRNA to NOR chromatin is UBF-dependent and occurs independent of transcription in human cells. *Genes Dev.*, **21**, 2041–2054.
73. Freed, E.F., Bleichert, F., Dutca, L.M. and Baserga, S.J. (2010) When ribosomes go bad: diseases of ribosome biogenesis. *Mol. Biosyst.*, **6**, 481–493.
74. Qu, J., Wang, D. and Grosskreutz, C.L. (2010) Mechanisms of retinal ganglion cell injury and defense in glaucoma. *Exp. Eye Res.*, **91**, 48–53.
75. Nickells, R.W., Semaan, S.J. and Schlamp, C.L. (2008) Involvement of the Bcl2 gene family in the signaling and control of retinal ganglion cell death. *Prog. Brain Res.*, **173**, 423–435.
76. Chi, Z.L., Yasumoto, F., Sergeev, Y., Minami, M., Obazawa, M., Kimura, I., Takada, Y. and Iwata, T. (2010) Mutant WDR36 directly affects axon

growth of retinal ganglion cells leading to progressive retinal degeneration in mice. *Hum. Mol. Genet.*, **19**, 3806–3815.
77. Fuchshofer, R., Birke, M., Welge-Lüssen, U., Kook, D. and Lütjen-Drecoll, E. (2005) Transforming growth factor-beta 2 modulated extracellular matrix component expression in cultured human optic nerve head astrocytes. *Invest. Ophthalmol. Vis. Sci.*, **46**, 568–578.
78. Tamm, E.R., Siegner, A., Baur, A. and Lütjen-Drecoll, E. (1996) Transforming growth factor-β1 induces α-smooth muscle-actin expression in cultured human and monkey trabecular meshwork. *Exp. Eye Res.*, **62**, 389–397.
79. Ohlmann, A., Seitz, R., Braunger, B., Seitz, D., Bosl, M.R. and Tamm, E.R. (2010) Norrin promotes vascular regrowth after oxygen-induced retinal vessel loss and suppresses retinopathy in mice. *J. Neurosci.*, **30**, 183–193.
80. Fuchshofer, R., Yu, A.L., Teng, H.H., Strauss, R., Kampik, A. and Welge-Lussen, U. (2009) Hypoxia/reoxygenation induces CTGF and PAI-1 in cultured human retinal pigment epithelium cells. *Exp. Eye Res.*, **88**, 889–899.
81. Tamm, E.R., Russell, P., Johnson, D.H. and Piatigorsky, J. (1996) Human and monkey trabecular meshwork accumulate alpha B-crystallin in response to heat shock and oxidative stress. *Invest. Ophthalmol. Vis. Sci.*, **37**, 2402–2413.
82. Hadjiolova, K.V., Nicoloso, M., Mazan, S., Hadjiolov, A.A. and Bachellerie, J.P. (1993) Alternative pre-rRNA processing pathways in human cells and their alteration by cycloheximide inhibition of protein synthesis. *Eur. J. Biochem.*, **212**, 211–215.